J. Fluid Mech. (2014), *vol.* 758, R4, doi:10.1017/jfm.2014.552



JFM RAPIDS
journals.cambridge.org/rapids

Transient growth in strongly stratified shear layers

A. K. Kaminski[1], C. P. Caulfield[2,1] and J. R. Taylor[1,†]

[1]Department of Applied Mathematics and Theoretical Physics, University of Cambridge, Wilberforce Road, Cambridge CB3 0WA, UK

[2]BP Institute, University of Cambridge, Madingley Rise, Madingley Road, Cambridge CB3 0EZ, UK

(Received 27 June 2014; revised 12 August 2014; accepted 18 September 2014; first published online 7 October 2014)

We investigate numerically transient linear growth of three-dimensional perturbations in a stratified shear layer to determine which perturbations optimize the growth of the total kinetic and potential energy over a range of finite target time intervals. The stratified shear layer has an initial parallel hyperbolic tangent velocity distribution with Reynolds number $Re = U_0 h/\nu = 1000$ and Prandtl number $\nu/\kappa = 1$, where ν is the kinematic viscosity of the fluid and κ is the diffusivity of the density. The initial stable buoyancy distribution has constant buoyancy frequency N_0, and we consider a range of flows with different bulk Richardson number $Ri_b = N_0^2 h^2/U_0^2$, which also corresponds to the minimum gradient Richardson number $Ri_g(z) = N_0^2/(\mathrm{d}U/\mathrm{d}z)^2$ at the midpoint of the shear layer. For short target times, the optimal perturbations are inherently three-dimensional, while for sufficiently long target times and small Ri_b the optimal perturbations are closely related to the normal-mode 'Kelvin–Helmholtz' (KH) instability, consistent with analogous calculations in an unstratified mixing layer recently reported by Arratia *et al.* (*J. Fluid Mech.*, vol. 717, 2013, pp. 90–133). However, we demonstrate that non-trivial transient growth occurs even when the Richardson number is sufficiently high to stabilize all normal-mode instabilities, with the optimal perturbation exciting internal waves at some distance from the midpoint of the shear layer.

Key words: instability, ocean processes, stratified flows

1. Introduction

Turbulent mixing in the stably stratified ocean interior is thought to play an important role in setting the vertical density structure and global distributions of tracers such as carbon and nutrients that are important to climate and biogeochemical

† Email address for correspondence: J.R.Taylor@damtp.cam.ac.uk

© Cambridge University Press 2014

https://doi.org/10.1017/jfm.2014.552 Published online by Cambridge University Press

cycles (Wunsch & Ferrari 2004; Kuhlbrodt *et al.* 2007). The turbulent eddies responsible for mixing in the ocean interior are typically no larger than several metres, much smaller than the grid spacing in ocean circulation models. As a result, the physics leading to localized dissipation of energy and mixing of tracers must be parameterized (Garrett 2003).

One mechanism believed to trigger small-scale mixing in the ocean is Kelvin–Helmholtz (KH) instability. The stability of a stratified parallel shear flow to KH instability can be classified using the local gradient Richardson number, $Ri_g(z) = N^2/S^2$, where N is the buoyancy frequency and S the vertical shear, which in general vary with the vertical coordinate z. The Miles–Howard stability theorem states that two-dimensional inviscid steady stably stratified parallel flows are stable to infinitesimal normal-mode perturbations if the gradient Richardson number $Ri_g(z) > 1/4$ everywhere in the flow, with $Ri_g(z) < 1/4$ for some z a necessary but not sufficient condition for instability (Drazin & Reid 2004).

Mixing parameterizations in ocean models often assume that turbulent mixing is reduced or eliminated when the Richardson number is larger than a critical value. However, turbulence has been observed in more strongly stratified flows using numerical simulations (e.g. Riley & de Bruyn Kops 2003; Lindborg 2006), laboratory experiments (e.g. Spedding, Browand & Fincham 1996; Augier *et al.* 2014), and ocean observations (e.g. Mack & Schoeberlein 2004; Polzin & Ferrari 2004). These results do not contradict the Miles–Howard theorem, which strictly applies to linear normal-mode perturbations to a steady, inviscid parallel stratified shear flow, but they do call into question conventional uses of the Miles–Howard theorem beyond its strict regime of applicability. Indeed, these observations rather suggest that mechanisms other than conventional KH instability might be important in triggering transition to turbulence in stratified fluids.

One of the over-arching objectives of our work is to determine whether there are alternative candidate mechanisms which lead to turbulence other than classic linear instabilities. Before exploring the nonlinear evolution and the transition to turbulence, it is important to identify these alternative candidate mechanisms. In the present study, we will examine whether infinitesimal linear perturbations to a stratified shear flow can grow when $Ri_g(z) > 1/4$ everywhere. Although we will not address nonlinearity or mixing directly, describing the evolution of linear perturbations is an essential first step towards understanding the development of turbulence in strongly stratified fluids.

Transient linear growth is one alternative candidate mechanism for turbulence transition in a flow with $Ri_g > 0.25$ everywhere. Recall that the Miles–Howard theorem applies to normal-mode perturbations. However, due to the non-normality of the Navier–Stokes operator, it is possible that, over a finite horizon time T, other perturbations may exhibit larger energy gain (see the review of Schmid 2007). As demonstrated by Arratia, Caulfield & Chomaz (2013), the optimal perturbation with largest gain in an unstratified shear layer tends towards the KH instability as $T \to \infty$. It is thus natural to ask how stratification might modify this observation, building on the previous calculations by Tearle (2004), who considered optimal perturbation growth in stratified flow using an approach based on linear algebra.

As discussed by Schmid (2007) it is actually often more convenient to identify the optimal perturbations through the solution of a variational problem using the so-called 'direct–adjoint looping' (DAL) method. Here, as a first step towards our over-arching research objectives, we seek linear optimal perturbations of a stratified shear flow using this method. Our primary aims in this paper are twofold. First, we wish to explore the properties of linear optimal perturbations, their connection to the

https://doi.org/10.1017/jfm.2014.552 Published online by Cambridge University Press

KH instability, and the modifying effect of stratification on their dynamics. Second, and more importantly, we wish to investigate whether there can be substantial linear transient growth for $Ri_g(z) > 1/4$ everywhere, by analogy with the observations of Constantinou & Ioannou (2011). They observed transient growth in a flow restricted to two dimensions with a 'sharp' density interface for wavenumbers outside the range predicted to be unstable to the travelling wave instability originally discussed by Holmboe (1962). We wish to go substantially further, in that we wish to determine if non-trivial transient growth can occur in a region of parameter space where no linear instabilities can occur. From experience in unstratified flows where there are no linear instabilities (e.g. plane Couette flow, the flow of a viscous fluid between two horizontal plates moving at fixed finite relative velocities), it is certainly conceivable that transient perturbations can exist, and it is likely that they are inherently three-dimensional. The evidence from unstratified flows is that such transient perturbations can play central roles in 'subcritical' transition when they reach finite amplitude, as discussed recently by Kerswell, Pringle & Willis (2014).

The remainder of this paper will proceed as follows. In § 2 we briefly describe the (linear) DAL method for finding the most rapidly growing linear modes for a stratified shear layer, which we will then use in § 3 to address our primary aims, in particular by finding non-trivial gains when $Ri_g(z) > 1/4$. In § 4, we draw some conclusions and discuss future directions.

2. Theory

We consider a parallel shear layer $\boldsymbol{U}^* = (U^*(z^*), 0, 0)$ with a constant gradient in buoyancy $B^*(z^*)$, described by

$$U^*(z^*) = U_0^* \left[\tanh\left(\frac{z^*}{h^*} - \frac{L_z^*}{4h^*} \right) - \tanh\left(\frac{z^*}{h^*} - \frac{3L_z^*}{4h^*} \right) - 1 \right], \quad B^*(z^*) = N_0^{*2} z^*, \quad (2.1a,b)$$

where half the shear layer thickness h^*, half the velocity difference U_0^*, and the buoyancy frequency N_0^* have been used to scale dimensional quantities (denoted with an asterisk). Time is scaled by the advective time scale h^*/U_0^* and buoyancy is scaled by $N_0^{*2} h^*$. In non-dimensional form (2.1) can be written

$$U(z) = \tanh\left(z - \frac{L_z}{4} \right) - \tanh\left(z - \frac{3L_z}{4} \right) - 1, \quad B(z) = z, \quad z = z^*/H^*. \quad (2.2a,b)$$

We consider this double shear layer structure so that periodic boundary conditions can be imposed at $z = 0$, L_z, with L_z sufficiently large so that each shear layer evolves essentially independently and identically, up to the sign of the streamwise component of velocity. Henceforth, we describe the dynamics of the lower shear layer alone in the region $0 \leqslant z \leqslant L_z/2$.

Key non-dimensional parameters describing the flow are the Reynolds number, $Re = U_0^* h^*/\nu^*$, the Prandtl number, $Pr = \nu^*/\kappa^*$ (ν^* being the kinematic viscosity and κ^* the diffusivity of density), and the bulk Richardson number, $Ri_b = N_0^{*2} h^{*2}/U_0^{*2}$. For the basic state, $Ri_g(z) \approx Ri_b \cosh^4(z - L_z/4)$. The minimum $Ri_g(z_c) = Ri_b$ occurs at the centre of the shear layer, $z_c = L_z/4$. The flow is assumed to be Boussinesq and incompressible.

We are interested in the linear evolution of small amplitude perturbations to (2.2), denoted $\boldsymbol{u}(x, y, z, t)$ and $b(x, y, z, t)$. In particular, we seek the initial conditions $\boldsymbol{u}_0(\boldsymbol{x})$ and $b_0(\boldsymbol{x})$ leading to maximum perturbation energy growth over a finite-time

https://doi.org/10.1017/jfm.2014.552 Published online by Cambridge University Press

interval T, where the total perturbation energy is a sum of the kinetic energy and potential energy of the perturbation, i.e.

$$E = \frac{\langle \boldsymbol{u}, \boldsymbol{u}\rangle + Ri_b\langle b, b\rangle}{2} = K + P, \tag{2.3}$$

and angled brackets denote an appropriate inner product, e.g. $\langle \boldsymbol{u}, \boldsymbol{v}\rangle \equiv 1/V \int_V \boldsymbol{u}\cdot\boldsymbol{v}\mathrm{d}V$, and V is the domain volume. We wish to find the maximum perturbation energy gain, $G(T) = E(T)/E_0$, where $E_0 = (\langle \boldsymbol{u}_0, \boldsymbol{u}_0\rangle + Ri_b\langle b_0, b_0\rangle)/2$ is the energy of the initial perturbation, which without loss of generality can be set to one since we consider a linear problem, and $E(T)$ is the perturbation energy at the final time $t = T$.

The maximum gain $G(T)$ can be found using a now-conventional DAL variational method (see Schmid 2007) similar to that used by Arratia *et al.* (2013) but generalized to stratified flow. The linearized Navier–Stokes equations, the linearized equation for conservation of buoyancy, mass continuity, and the initial conditions of the flow at $t = 0$ are imposed as constraints, using appropriate Lagrange multipliers, in an augmented Lagrangian where the objective functional is the total perturbation gain at the target time T, i.e.

$$\begin{aligned}\mathscr{L} = {} & \frac{\langle \boldsymbol{u}(T), \boldsymbol{u}(T)\rangle + Ri_b\langle b(T), b(T)\rangle}{\langle \boldsymbol{u}_0, \boldsymbol{u}_0\rangle + Ri_b\langle b_0, b_0\rangle} \\ & - \left[\partial_t u_i + u_j\partial_j U_i + U_j\partial_j u_i + \partial_i p - Re^{-1}\partial_j\partial_j u_i - Ri_b b\delta_{i3},\, v_i\right] \\ & - \left[\partial_t b + u_j\partial_j B + U_j\partial_j b - (RePr)^{-1}\partial_j\partial_j b,\, \varphi\right] - \left[\partial_i u_i,\, q\right] \\ & - \langle u_i(0) - u_{0i},\, v_{0i}\rangle - \langle b(0) - b_0,\, \varphi_0\rangle \end{aligned} \tag{2.4}$$

and $[\boldsymbol{u}, \boldsymbol{v}] \equiv \int_0^T \langle \boldsymbol{u}, \boldsymbol{v}\rangle \mathrm{d}t$. Taking variations of this quantity with respect to the Lagrange multipliers $\boldsymbol{v}(\boldsymbol{x}, t)$, $\varphi(\boldsymbol{x}, t)$ and $q(\boldsymbol{x}, t)$, we recover the 'forward' or 'direct' evolution equations, i.e. the linearized Navier–Stokes equations, conservation of buoyancy, and mass continuity. Variations of $\mathscr{L}$ with respect to $\boldsymbol{v}_0(\boldsymbol{x})$ and $\varphi_0(\boldsymbol{x})$ give the definition of the initial conditions $\boldsymbol{u}_0(\boldsymbol{x})$ and $b_0(\boldsymbol{x})$, where the subscript '0' indicates that these quantities refer to the initial conditions of the flow.

The Lagrange multipliers $\boldsymbol{v}$, φ and q can be calculated by taking variations of (2.4) with respect to the physical or 'direct' variables $\boldsymbol{u}$, b and p, and setting the result equal to zero to obtain the 'adjoint' equations. These equations describe the evolution of the 'adjoint velocity' $\boldsymbol{v}$, 'adjoint buoyancy' φ, and 'adjoint pressure' q,

$$\frac{\partial v_i}{\partial t} = v_j\frac{\partial U_j}{\partial x_i} - \frac{\partial}{\partial x_j}(U_j v_i) + \varphi\frac{\partial B}{\partial x_i} - \frac{\partial q}{\partial x_i} - \frac{1}{Re}\frac{\partial^2 v_i}{\partial x_j^2}, \tag{2.5}$$

$$\frac{\partial \varphi}{\partial t} = -\frac{\partial}{\partial x_j}(U_j\varphi) - Ri_b v_3 - \frac{1}{RePr}\frac{\partial^2\varphi}{\partial x_j^2}, \tag{2.6}$$

$$\frac{\partial v_i}{\partial x_i} = 0. \tag{2.7}$$

The adjoint equations act as sensitivities to the governing equations for the perturbations, and are well-posed when integrated backwards in time (Schmid 2007; Luchini & Bottaro 2014). Along with (2.5) and (2.6), which must be satisfied for all times $0 \leqslant t \leqslant T$, variations of (2.4) with respect to $\boldsymbol{u}$ and b also yield compatibility conditions which must be satisfied at the target time T:

$$\left(\frac{u_i}{E_0} - v_i\right)\bigg|_{t=T} = 0 \quad \text{and} \quad \left(\frac{Ri_b b}{E_0} - \varphi\right)\bigg|_{t=T} = 0. \tag{2.8a,b}$$

https://doi.org/10.1017/jfm.2014.552 Published online by Cambridge University Press

Ri_b	T	L_x	L_y	L_z	N_x	N_y	N_z
0.12	1, 2	10.8	15.0	60.0	64	64	512
0.12	5, 10, 15, 20, 30	21.6	30.0	60.0	64	64	512
0.20, 0.25, 0.30, 0.50	1, 2	9.44	15.0	60.0	64	64	512
0.20, 0.25, 0.30, 0.50	5, 10, 15, 20, 30	18.9	30.0	60.0	64	64	512

TABLE 1. Physical and numerical parameters used for the calculation of optimal perturbations. Lengths have been normalized by half the shear layer thickness h^*.

The variational approach requires that variations of (2.4) with respect to the initial perturbations $\boldsymbol{u}_0$ and b_0 be zero for maximum perturbation energy gain, implying

$$v_{0i} - \frac{u_{0i}E(T)}{E_0^2} = 0, \quad \varphi_0 - \frac{Ri_b b_0 E(T)}{E_0^2} = 0. \tag{2.9a,b}$$

As discussed in more detail in Rabin, Caulfield & Kerswell (2012), an appropriate convergence criterion is then to consider the normalized residual,

$$R_n = \frac{\langle \delta\mathscr{L}/\delta\boldsymbol{u}_0, \delta\mathscr{L}/\delta\boldsymbol{u}_0\rangle + \langle \delta\mathscr{L}/\delta b_0, \delta\mathscr{L}/\delta b_0\rangle}{\langle \boldsymbol{v}(0), \boldsymbol{v}(0)\rangle + \langle \varphi(0), \varphi(0)\rangle/Ri_b}. \tag{2.10}$$

Optimal perturbations are then found using an iterative procedure. The flow is initialized with random noise and marched forward in time using the direct equations until the target time T. At $t = T$, the direct physical variables are used to initialize the adjoint variables using the compatibility conditions (2.8). The adjoint variables are then marched backward in time using (2.5)–(2.7) until $t = 0$. The initial condition is then updated. The direct–adjoint loop is repeated until the flow converges to the optimal initial condition. Here, iterations are continued until $R_n < 10^{-4}$.

To implement this procedure, we have written linearized direct and adjoint solvers connected by a time-looping wrapper. The numerical method uses a combined three-step third-order Runge–Kutta–Wray/Crank–Nicolson solver with a pressure projection method (Taylor 2008). As the domain is triply periodic, spatial derivatives are computed using the pseudo-spectral method. Power iteration is used to update the initial condition. The calculated linear optimal perturbations, in the absence of stratification, agree well with those found by Arratia *et al.* (2013).

3. Results

Linear optimal perturbations are calculated for flows with background profiles given by (2.2), with $Pr = 1$ and $Re = 1000$. Physical and numerical parameters are given in table 1. As the equations of motion are solved in non-dimensional form, Ri_b is varied directly rather than by varying either shear or stratification individually. For $Ri_b < 1/4$, for which there is a predicted most unstable normal mode of linear theory, the streamwise domain size, L_x, is set to the wavelength associated with the most unstable mode for short target times ($T \leqslant 2$), and to twice that wavelength for longer target times ($T > 2$). For larger values of Ri_b, for which there is no predicted unstable normal mode, the domain is set to the same size as in the $Ri_b = 0.20$ case. The vertical domain size, L_z, is 60 times the shear layer half-width, which is sufficiently large such that the two shear layers will not interact with each other or the edges of

https://doi.org/10.1017/jfm.2014.552 Published online by Cambridge University Press

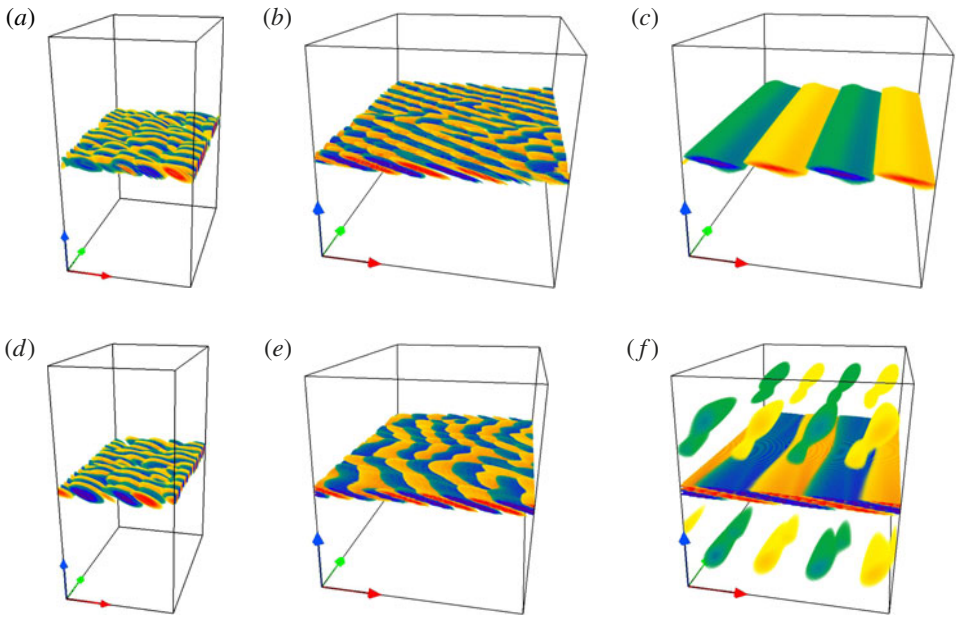


FIGURE 1. Vertical velocities associated with the linear optimal perturbations. (*a–c*) $Ri_b = 0.12$ and $T = 1, 5, 20$, respectively. (*d–f*) $Ri_b = 0.50$ and $T = 1, 5, 20$, respectively. The red, green and blue arrows denote the x, y and z directions, and the yellow/red and green/blue colours denote positive and negative values of vertical velocity. Only the lower shear layer is shown here.

the computational domain. To confirm that the two layers are not interacting, several cases were run with $L_z = 80.0$; similar results were obtained for the larger domain. Henceforth, only one shear layer will be shown, but statistics are averaged across both shear layers. Higher vertical resolution is used in order to resolve the relatively thin shear layers.

As illustrated in figure 1, the linear optimal perturbations for this flow take the form of an array of perturbations tilted against the background shear, confined to the shear layers. In general, shorter target times have three-dimensional optimal perturbations with high wavenumbers in both the x and y directions, as is apparent from the horizontal spectra of the optimal perturbations, shown in figure 2. Conversely, the optimal perturbations associated with longer target times have smaller wavenumbers in the spanwise direction, and become two-dimensional by $T \approx 15$–20, as shown in the bottom panels of figure 2. The rolls are also more strongly tilted against the shear for larger T, similarly to the unstratified case as observed by Arratia *et al.* (2013) and in agreement with the linear optimal perturbations found by Tearle (2004) using a different (linear algebra-based) technique. As the flow evolves, the primarily spanwise rolls associated with the optimal perturbation are tilted into and against the prevailing mean shear, reaching a state in which they are approximately vertical near the target time, in which they have been effectively amplified by the mean shear via the action of the Reynolds stress. This evolution is consistent with transient growth via the Orr mechanism in unstratified flows (Orr 1907), although, as noted by Arratia *et al.* (2013), the actual dynamics of the transient growth is inherently three-dimensional, and should thus be thought of as a hybrid of the Orr mechanism and the 'lift-up' or

https://doi.org/10.1017/jfm.2014.552 Published online by Cambridge University Press

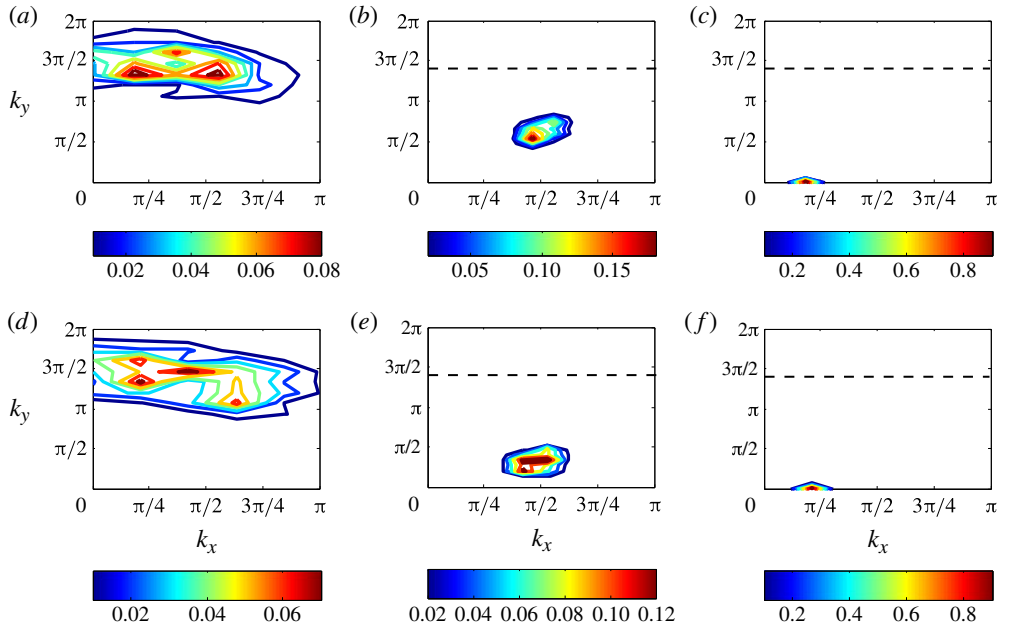


FIGURE 2. Horizontal structure of optimal perturbations in wavenumber space for different target times. (*a–c*) $Ri_b = 0.12$, $T = 1$, 5, 20, respectively. (*d–f*) $Ri_b = 0.50$, $T = 1$, 5, 20, respectively. Contours denote the fraction of initial perturbation energy for each combination of wavenumbers (k_x, k_y). The horizontal dashed line indicates the limits of the spectral data in the y direction (i.e. two-thirds the Nyquist wavenumber $k_{y,Nyq} = N_y\pi/L_y$). The limit of spectral resolution is outside the plotted area in panels (*a*) and (*d*).

tilting mechanism which leads to algebraic growth in primarily streamwise vortical perturbations (Ellingsen & Palm 1975; Landahl 1980).

For long target times ($T > 20$) and $Ri_b < 1/4$, the optimal perturbation is two-dimensional with a horizontal wavelength matching that predicted by the Taylor–Goldstein equation, in agreement with the findings of Tearle (2004) and Arratia *et al.* (2013). The computed optimal perturbation should approach the predicted most unstable normal mode at late target times, although it can still have larger gain than the normal mode due to augmentation by the Orr mechanism at early times. For longer target times, the optimal perturbations for higher Ri_b are no longer strictly localized inside the shear layer, although they are still close to two-dimensional. While there are still rolls tilted against the mean shear found in the shear layers themselves, distinct perturbations can be seen outside of the shear layer (figure 1*f*). The vertical velocity and buoyancy associated with the perturbations outside the shear layer are approximately 90° out of phase (not shown), consistent with the structure of a linear internal gravity wave.

Next, we turn our attention to the perturbation energy gain at the target time, $G(T)$. As can be seen in figure 3, $O(10–100)$ energy growth may be observed for intermediate target times, even for flows expected to be stable to normal-mode instability ($Ri_b > 1/4$), as in Farrell & Ioannou (1993*b*) and Constantinou & Ioannou (2011). For flows predicted to be linearly stable by the Miles–Howard theorem, $G(T)$ reaches a maximum value at an intermediate target time, T, before decreasing for higher T. The maximum value of the gain is highly sensitive to the bulk Richardson number, with $G(T = 15) \simeq 47$ when $Ri_b = 0.3$ and $G(T = 15) \simeq 13$ when $Ri_b = 0.5$.

https://doi.org/10.1017/jfm.2014.552 Published online by Cambridge University Press

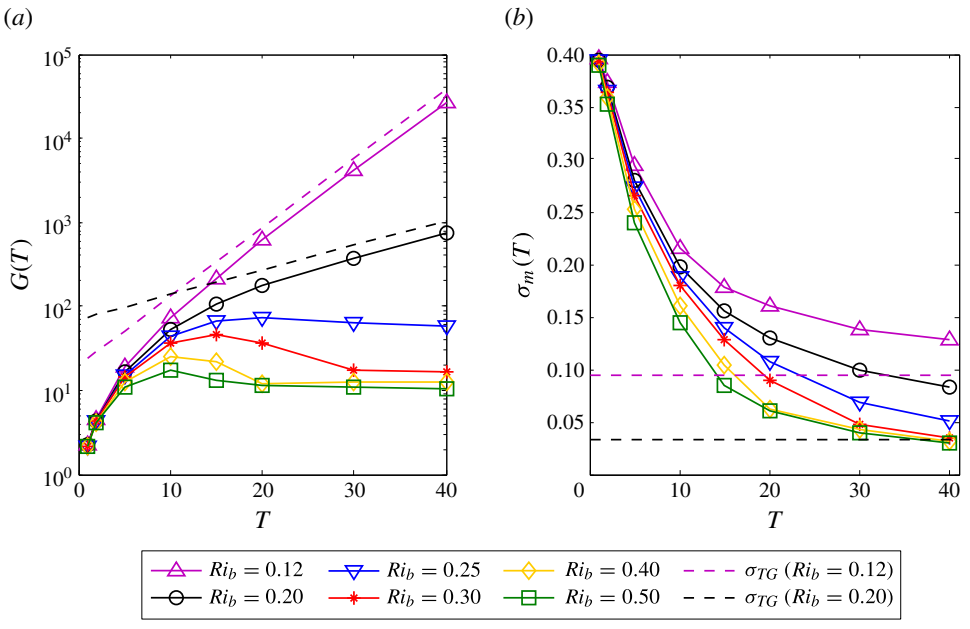


FIGURE 3. Maximum perturbation gain and mean growth rate for the flow described by (2.2), for several values of Ri_b. (*a*) Gain, $G(T)$. (*b*) Mean growth rate, σ_m.

The mean growth rates $\sigma_m = \ln G(T)/(2T)$, averaged over the time interval 0 to T, are found to be highest for short times and decrease with increasing target times, suggesting strong transient growth is possible at short times. For late target times ($T = 30$), the mean growth rates observed for $Ri_b = 0.12$ and $Ri_b = 0.20$ are still higher than the growth rates predicted by the viscous Taylor–Goldstein equation, denoted by σ_{TG} in figure 3, although the growth rates tend towards the predicted values with increasing target time T. The enhanced mean growth at large T is further evidence of initial growth due to a hybrid combination of the Orr mechanism and the lift-up mechanism, analogously to the unstratified results of Arratia *et al.* (2013).

The linear evolution of the optimal perturbations, both before and after the target time, can be examined further by considering the temporal evolution of the perturbation energy gain, shown by the solid lines in figure 4(*a–c*). The dashed lines show the contribution of the perturbation kinetic energy to the total, with the remainder due to potential energy. Figure 4(*a–c*) shows that the maximum perturbation energy gain obtained by the optimal perturbations need not necessarily occur directly at the target time; indeed, in many of the scenarios shown, the peak in perturbation energy occurs well after $t = T$. The potential energy is a larger fraction of the total energy in the more strongly stratified flows, as expected.

The evolution of total perturbation energy E, potential energy P, and kinetic energy K, as defined in (2.3), are governed by

$$\frac{\mathrm{d}E}{\mathrm{d}t} = -\overline{u_1 u_3}U' - (\mathscr{E}_K + \mathscr{E}_P), \quad \frac{\mathrm{d}K}{\mathrm{d}t} = -\overline{u_1 u_3}U' + Ri_b\overline{u_3 b} - \mathscr{E}_K, \quad \frac{\mathrm{d}P}{\mathrm{d}t} = -Ri_b\overline{u_3 b} - \mathscr{E}_P, \tag{3.1a–c}$$

where the prime denotes differentiation and the overbar denotes a spatial average over the computational domain. The values $\mathscr{E}_K = \overline{\partial_j u_i \partial_j u_i}/Re$ and $\mathscr{E}_P = Ri_b\overline{\partial_j b \partial_j b}/(RePr)$ are positive-definite quantities associated with dissipation of the kinetic and potential

https://doi.org/10.1017/jfm.2014.552 Published online by Cambridge University Press

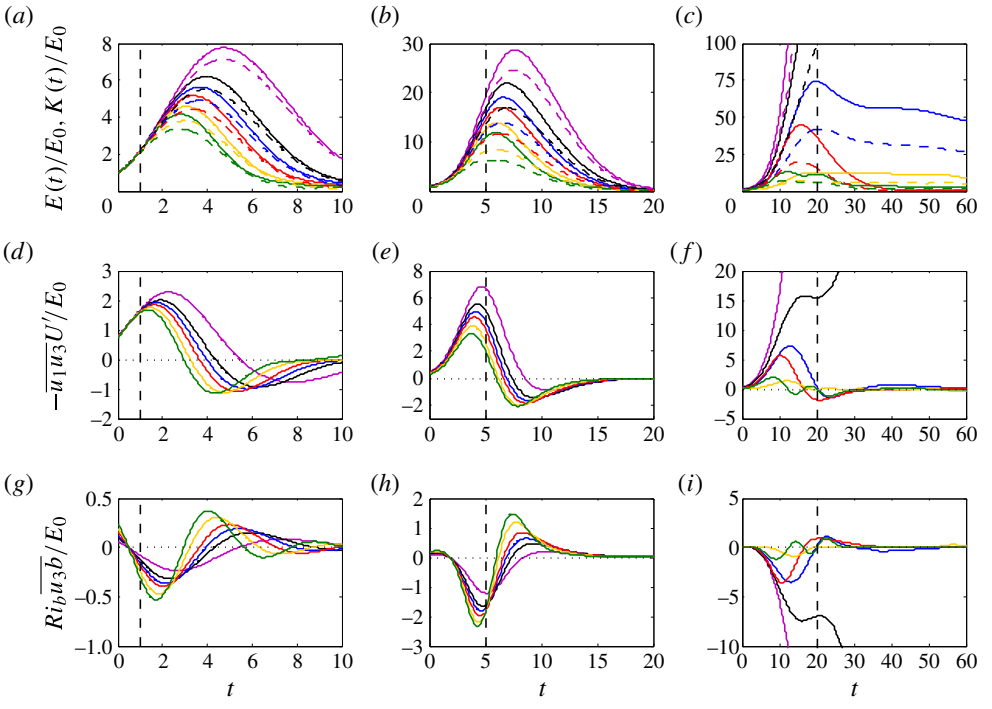


FIGURE 4. (*a–c*) Linear evolution of perturbation gain $G(t)$ (solid) and kinetic energy $K(t)/E_0$ (dashed), for $T = 1, 5, 20$, respectively. (*d–f*) Shear production, $-\overline{u_1u_3}U'$, for $T = 1, 5, 20$, respectively. (*g–i*) Vertical buoyancy flux, $Ri_b\overline{u_3b}$, for $T = 1, 5, 20$, respectively. Vertical dashed lines denote the target time. Colours are as in figure 3.

energy, while $-\overline{u_1u_3}U'$ and $Ri_b\overline{u_3b}$ are the shear production and vertical buoyancy flux, respectively (cf. Farrell & Ioannou 1993*b*).

Prior to the maximum in perturbation energy in cases with $T = 1$ and $T = 5$, the shear production is the dominant source of perturbation energy (figure 4*d–e*), and the rolls are tilted against the mean shear during this time. However, the vertical buoyancy flux changes sign during this period. While $Ri_b\overline{u_3b} > 0$ at very early times, corresponding with conversion of energy from potential into kinetic energy, as the perturbation energy continues to grow, the buoyancy flux changes sign and kinetic energy is converted back into potential energy (figure 4*g–h*).

At the time when $G(t)$ is a maximum (i.e. $\mathrm{d}E/\mathrm{d}t = 0$), which occurs after the target time for both $T = 1$ and 5, the rolls are nearly vertical and the shear production and buoyancy flux are still positive. Shortly after this maximum the shear production and buoyancy flux change sign. The negative shear production is associated with the alignment of the rolls with the mean shear, with kinetic energy being converted from the perturbations back into the mean flow. The evolution of perturbation energy observed here is similar to that seen by Farrell & Ioannou (1993*b*).

For the small target time $T = 1$, figure 4(*a*) shows that the perturbation energy growth is associated with kinetic energy. The shear production and vertical buoyancy flux peak after the target time. For $T = 5$, while the flow evolution follows a similar pattern, potential energy makes up a larger proportion of the overall perturbation energy at $t = T$ (figure 4*b*), especially for higher values of Ri_b, and shear production and buoyancy flux peak slightly before the target time (figure 4*e*,*h*).

https://doi.org/10.1017/jfm.2014.552 Published online by Cambridge University Press

Conversely, for long target times ($T = 20$), the perturbations are two-dimensional (figure 2*c*,*f*), with potential energy making up a substantial fraction of the total perturbation energy. Figures 4(*c*), (*f*) and (*i*) show clear qualitative changes in perturbation evolution when compared with those for shorter target times. The flows with $Ri_b < 1/4$ exhibit exponential growth, for which instantaneous growth rates at later times are comparable to those predicted by linear theory. While the growth for $Ri_b = 0.12$ appears to be that of a modal instability, the growth for $Ri_b = 0.20$ is not purely exponential, and some transient growth is apparent around $t = 20$. The flow with $Ri_b = 0.25$ is the only case where the peak in total perturbation energy exactly coincides with the target time T, and the energy in this case remains elevated for $t > T$. For $Ri_b = 0.30$, the flow appears to follow a similar evolution to the flows at shorter target times, although the peak in total perturbation energy occurs well before the target time.

For more strongly stratified flows, there is a clear change in perturbation evolution: the perturbation energy remains elevated at longer times and oscillations in the perturbation energy, shear production and vertical buoyancy flux are observed. The period of these oscillations is comparable to the buoyancy period, $\tau_b = 2\pi/\sqrt{Ri_b}$. This is indicative of a shift to a mode with energy in both tilted rolls in the shear layer and the internal wave structure outside of the shear layer, as shown in figure 1(*f*), with a high fraction of potential energy. The oscillations in the buoyancy flux in this case indicate that energy is being periodically converted between kinetic and potential energy.

4. Discussion

Linear optimal perturbations maximizing finite-time energy gain in a stratified shear layer have been computed for a variety of Richardson numbers, corresponding to KH-stable and KH-unstable flow configurations, using a now-conventional variational technique which we refer to as the DAL method. The computed optimal perturbations may undergo O(10–100) energy growth even when $Ri_b > 1/4$. There is good agreement between the perturbations found here and those found by Farrell & Ioannou (1993*b*), Tearle (2004) and Arratia *et al.* (2013).

The growth, structure, and energetics of the optimal perturbations at short target times are not strongly dependent on stratification, implying that the same physical mechanism might be responsible for the growth across all Ri_b. In unstratified shear flow, Farrell & Ioannou (1993*a*) and Arratia *et al.* (2013) identified a mechanism that combines aspects of the Orr mechanism, which leads to perturbation growth through the action of the Reynolds stress on largely spanwise vortical perturbations (Orr 1907), and the lift-up or tilting mechanism for algebraic growth of largely streamwise vortical perturbations (Ellingsen & Palm 1975; Landahl 1980). However, for later target times, where the optimal perturbations become increasingly two-dimensional and the potential energy plays a larger role, there is a shift away from this mechanism to one in which the growth is due to the interaction of the perturbations with the background shear and the conversion of energy between potential and kinetic energy (Farrell & Ioannou 1993*b*). For more strongly stratified flows, some of the perturbation energy is found in internal wave-like structures outside of the shear layer, allowing for increased perturbation energy due to the high potential energy of the waves. Conservation of wave action (Bretherton & Garrett 1969) would suggest that perturbations will grow in amplitude as they become tilted upright by the shear flow. However, the assumption of a slowly varying background flow is not valid in our case, and the changes in

https://doi.org/10.1017/jfm.2014.552 Published online by Cambridge University Press

amplitude based on the WKB theory of Bretherton & Garrett (1969) do not capture the qualitative dependence of gain on Richardson number and target time.

Given the large perturbation energy growth observed here, we believe that we have established that there are several 'candidates' for transition in a stratified shear flow which are not normal modes, both for flows with instabilities present, and also flows where the Miles–Howard theorem predicts linear stability. A natural question to ask is what the fate of these linear perturbation candidates would be if they were allowed to evolve in a fully nonlinear manner. Of particular interest are the cases for which the background flow is predicted to be stable to KH instability, i.e. the more strongly stratified flows. Although the predicted gain is modest for the flow with $Ri_b = 0.5$ ($G(T = 15) \simeq 13$), there is substantial gain evident for the flow with $Ri_b = 0.3$ ($G(T = 15) \simeq 47$). Since we did not optimize the gain over streamwise extent or target time T, for $Ri_b > 1/4$, it is entirely possible that the maximum such gain may actually be somewhat larger. Indeed, we conjecture that the transient growth observed when $Ri_b = 0.3$ may well be sufficient to allow for nonlinear effects to become significant, and lead to a 'stratified subcritical transition', possibly leading to enhanced dissipation and mixing of these flows.

This conjecture, and the more general question about the nonlinear fate of perturbations with these calculated 'optimal' structures, will be examined in future work, though recent research in unstratified flows (Kerswell *et al.* 2014) suggests that sequential combinations of such optimal perturbations can combine to great effect to lead to large perturbation growth, and hence potentially transition. Establishing that such candidate, transiently growing perturbations exist is an essential first step in identifying and describing such routes to transition not based around the development, saturation and ultimate break down of normal modes. We are encouraged that these new non-normal transiently growing perturbations may well be significant since the evidence of direct numerical simulations suggests that turbulence can arise in strongly stratified flows. This is the first evidence of which we are aware establishing the possibility of non-trivial perturbation growth in steady shear flows with $Ri_g > 1/4$ everywhere, thus opening the possibility for stratified subcritical transition to occur, which has the potential to remove the requirement for a 'strong' linear instability to be present to lead ultimately to mixing in a stably stratified shear flow.

Here, we have found and described the perturbations that optimize the total perturbation energy. However, this choice of norm is somewhat arbitrary, and there are other seminorm quantities which may be used in the linear framework (Foures, Caulfield & Schmid 2012). For instance, perturbations maximizing shear production, buoyancy flux, or kinetic or potential energy alone could be computed, with potentially different structures from those which maximize total perturbation energy. Large linear transient growth could thus be associated with different perturbation structures than those discussed above.

Finally, these conclusions may change for nonlinear optimal perturbations, i.e. those found using the full Navier–Stokes and buoyancy equations rather than the linearized forms considered here (Kerswell *et al.* 2014). This would introduce additional computational complexity, owing largely to the dependence of the adjoint equations on the forward variables; however, previous work has indicated that nonlinear optimal perturbations may attain higher gains than their linear counterparts for unstratified flow (Schmid 2007; Rabin *et al.* 2012; Luchini & Bottaro 2014).

Acknowledgements

The manuscript benefited from the helpful comments of three anonymous reviewers. A.K.K. was supported by a NSERC doctoral scholarship. The research activity of

https://doi.org/10.1017/jfm.2014.552 Published online by Cambridge University Press

C.P.C. and J.R.T. was supported by EPSRC Programme Grant EP/K034529/1, entitled 'Mathematical Underpinning of Stratified Turbulence'.

References

ARRATIA, C., CAULFIELD, C. P. & CHOMAZ, J.-M. 2013 Transient perturbation growth in time-dependent mixing layers. *J. Fluid Mech.* **717**, 90–133.

AUGIER, P., BILLANT, P., NEGRETTI, M. E. & CHOMAZ, J.-M. 2014 Experimental study of stratified turbulence forced with columnar dipoles. *Phys. Fluids* **26** (4), 046603.

BRETHERTON, F. P. & GARRETT, C. J. R. 1969 Wavetrains in inhomogeneous moving media. *Proc. R. Soc. Lond.* A **302**, 529–554.

CONSTANTINOU, N. C. & IOANNOU, P. J. 2011 Optimal excitation of two-dimensional Holmboe instabilities. *Phys. Fluids* **23**, 074102.

DRAZIN, P. G. & REID, W. H. 2004 *Hydrodynamic Stability*, 2nd edn Cambridge University Press.

ELLINGSEN, T. & PALM, E. 1975 Stability of linear flow. *Phys. Fluids* **18** (4), 487–488.

FARRELL, B. F. & IOANNOU, P. J. 1993*a* Optimal excitation of three-dimensional perturbations in viscous constant shear flow. *Phys. Fluids* A **5** (6), 1390–1400.

FARRELL, B. F. & IOANNOU, P. J. 1993*b* Transient development of perturbations in stratified shear flow. *J. Atmos. Sci.* **50** (14), 2201–2214.

FOURES, D. P. G., CAULFIELD, C. P. & SCHMID, P. J. 2012 Variational framework for flow optimization using seminorm constraints. *Phys. Rev.* E **86**, 026306.

GARRETT, C. 2003 Mixing with latitude. *Nature* **422**, 477–478.

HOLMBOE, J. 1962 On the behaviour of symmetric waves in stratified shear layers. *Geophys. Publ.* **24**, 67–113.

KERSWELL, R. R., PRINGLE, C. C. T. & WILLIS, A. P. 2014 An optimization approach for analyzing nonlinear stability with transition to turbulence in fluids as an exemplar. *Rep. Prog. Phys.* **77**, 085901.

KUHLBRODT, T., GRIESEL, A., MONTOYA, M., LEVERMANN, A., HOFMANN, M. & RAHMSTORF, S. 2007 On the driving processes of the Atlantic meridional overturning circulation. *Rev. Geophys.* **45**, RG2001.

LANDAHL, M. T. 1980 A note on an algebraic instability of inviscid parallel shear flows. *J. Fluid Mech.* **98** (2), 243–251.

LINDBORG, E. 2006 The energy cascade in a strongly stratified fluid. *J. Fluid Mech.* **550**, 207–242.

LUCHINI, P. & BOTTARO, A. 2014 Adjoint equations in stability analysis. *Annu. Rev. Fluid Mech.* **46**, 493–517.

MACK, S. A. & SCHOEBERLEIN, H. C. 2004 Richardson number and ocean mixing: towed chain observations. *J. Phys. Oceanogr.* **34** (4), 736–754.

ORR, W. M. F. 1907 The stability or instability of the steady motions of a perfect liquid and of a viscous liquid. Part I: a perfect liquid. *Proc. R. Irish Acad.* A **27**, 9–68.

POLZIN, K. & FERRARI, R. 2004 Isopycnal dispersion in NATRE. *J. Phys. Oceanogr.* **34** (1), 247–257.

RABIN, S. M. E., CAULFIELD, C. P. & KERSWELL, R. R. 2012 Triggering turbulence efficiently in plane Couette flow. *J. Fluid Mech.* **712**, 244–272.

RILEY, J. J. & DE BRUYN KOPS, S. M. 2003 Dynamics of turbulence strongly influenced by buoyancy. *Phys. Fluids* **15** (7), 2047–2059.

SCHMID, P. J. 2007 Nonmodal stability theory. *Annu. Rev. Fluid Mech.* **39**, 129–162.

SPEDDING, G. R., BROWAND, F. K. & FINCHAM, A. M. 1996 Turbulence, similarity scaling and vortex geometry in the wake of a towed sphere in a stably stratified fluid. *J. Fluid Mech.* **314**, 53–103.

TAYLOR, J. R. 2008 Numerical simulations of the stratified oceanic bottom boundary layer. PhD thesis, University of California, San Diego.

TEARLE, M. O. 2004 Optimal perturbation analysis of stratified shear flow. PhD thesis, University of Colorado.

WUNSCH, C. & FERRARI, R. 2004 Vertical mixing, energy, and the general circulation of the oceans. *Annu. Rev. Fluid Mech.* **36**, 281–314.

https://doi.org/10.1017/jfm.2014.552 Published online by Cambridge University Press